GEOPHYSICS

Ambient noise Love wave attenuation tomography for the LASSIE array across the Los Angeles basin

Xin Liu[1], Gregory C. Beroza[1]*, Lei Yang[1,2]*, William L. Ellsworth[1]

The Los Angeles basin is located within the North America–Pacific plate boundary and contains multiple earthquake faults that threaten greater Los Angeles. Seismic attenuation tomography has the potential to provide important constraints on wave propagation in the basin and to provide supplementary information on structure in the form of the distribution of anelastic properties. On the basis of the amplitude information from seismic interferometry from the linear LASSIE array in the Los Angeles basin, we apply station-triplet attenuation tomography to obtain a 2D depth profile for the attenuation structure of the uppermost 0.6 km. The array crosses four Quaternary faults, three of which are blind. The attenuation tomography resolves strong attenuation (shear attenuation $Q_s \sim 20$) for the fault zones and is consistent with sharp boundaries across them.

INTRODUCTION

The Los Angeles basin proper is home to a population of ~3 million. The basin was formed in the late Neogene within the plate boundary zone between Pacific and North America plates (*1*, *2*). It is located south of the Big Bend of the San Andreas fault and accommodates a portion of the transform plate boundary motion through several regional/local faults. Among these faults, the right-lateral strike-slip Newport-Inglewood fault has clear surface expression and ruptured in a M_L 6.3 earthquake in 1933 (*3*). Three blind faults, the Los Alamitos, Norwalk, and lower Elysian Park thrust faults east of the Newport-Inglewood fault, do not have clear surface traces, and their locations and potential for earthquakes are poorly constrained. Traditionally, these blind faults are located using two indirect approaches: (i) offsets in subsurface interfaces imaged by seismic reflection surveys (*2*, *4*) or (ii) seismicity distribution around a moderate earthquake on that fault (*5*). The first approach is costly to carry out, may contain diffraction artifacts, and typically does not resolve the near-surface structure in Holocene sediments. The second approach relies on the sensitivity of seismic stations to small events in this urban environment and is of no use in the absence of detectable seismicity.

Seismic attenuation measures seismic wave amplitude decay due to absorption and scattering. Therefore, it is sensitive to the near-surface geological structure. It also provides crucial information for earthquake ground motion prediction. A fault zone is characterized by strong attenuation due to well-developed cracks and fractures (*6*). Attenuation structure has been studied using the spectral ratio method (*7*–*9*) and fault zone trapped waves (*10*), but with limited spatial resolution. For seismic noise interferometry, Weaver (*11*, *12*) and Liu *et al.* (*13*) have proposed attenuation inversion methods based on linear array of stations. Their goal is to cancel out the influences of noise sources, which are highly variable in space and time; however, they did not consider the effect of different Fresnel zone widths due to different interstation distances, which will be addressed in this paper. Love wave attenuation information has previously been extracted from higher-order noise correlations (*14*), and ambient noise data from USArray have been used for attenuation tomography at long periods across the continental United States based on Helmholtz tomography (*15*).

In this study, we use ambient seismic noise interferometry to infer the near-surface attenuation structure beneath the linear Los Angeles Syncline Seismic Interferometry Experiment (LASSIE) array (*16*) in the Los Angeles basin (Fig. 1). The attenuation tomography is based on different combinations of linear station triplets (*13*, *17*) in the LASSIE array. To suppress the effect of the azimuthal distribution of noise intensity, we add new constraints to the interstation distance ratios when taking amplitude ratios from two pairs of station within the triplet based on finite-frequency source kernels. Through our method, we find a strong correlation between high attenuation ($Q \sim 15$ to 25) and known fault traces in the Los Angeles basin and evidence of buried fault zone damage for blind faults.

RESULTS

Love wave attenuation tomography

We estimate the Love wave attenuation quality factor Q_L for 25 evenly spaced periods between 0.74 and 5.0 s. For each period, we first loop over each of the 42 stations as the virtual source and select the eligible station triplets with distances $x_{23} < 0.25x_{12}$, where the subscript 1 is the virtual source and the subscripts 2 and 3 represent two nearby receivers. Then, we estimate Q_{23} values for each triplet based on Eqs. 1 and 2 assuming that the site factors are similar for neighboring stations within the basin. The site effect is related to the amplification/deamplification of seismic wave amplitude due to the near-surface layers. Based on uncertainty quantification for the amplitude ratio, we only select the amplitude ratios (left-hand side of Eqs. 1 and 2) greater than six times their corresponding SD.

With the estimated Q_{23} values from different station triplets, we first discretize the horizontal axis parallel to the LASSIE array with a grid spacing of 0.3 km. We then carry out linear least-squares inversion by equating the path averaged attenuation $1/Q_{23}$ to the sum of the attenuation $1/Q$ contributions from different grid cells along the ray path between stations 2 and 3. The attenuation tomography for each period is computed by ridge regression with Tikhonov regularization terms and damping parameters selected using cross-validation (text S3).

[1]Department of Geophysics, Stanford University, Stanford, CA 94305, USA. [2]State Key Laboratory of Lithospheric Evolution, Institute of Geology and Geophysics, Chinese Academy of Sciences, Beijing 100029, China.
*Corresponding author. Email: beroza@stanford.edu (G.C.B.); yanglei@stanford.edu (L.Y.)

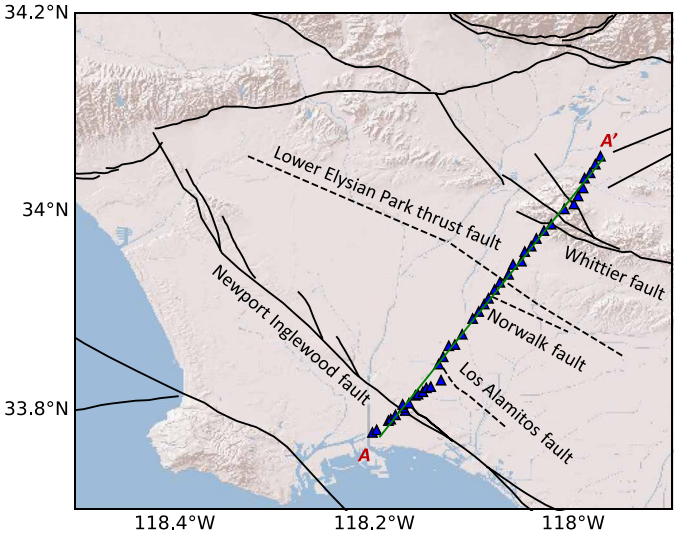

Fig. 1. Map of the LASSIE array and regional faults.

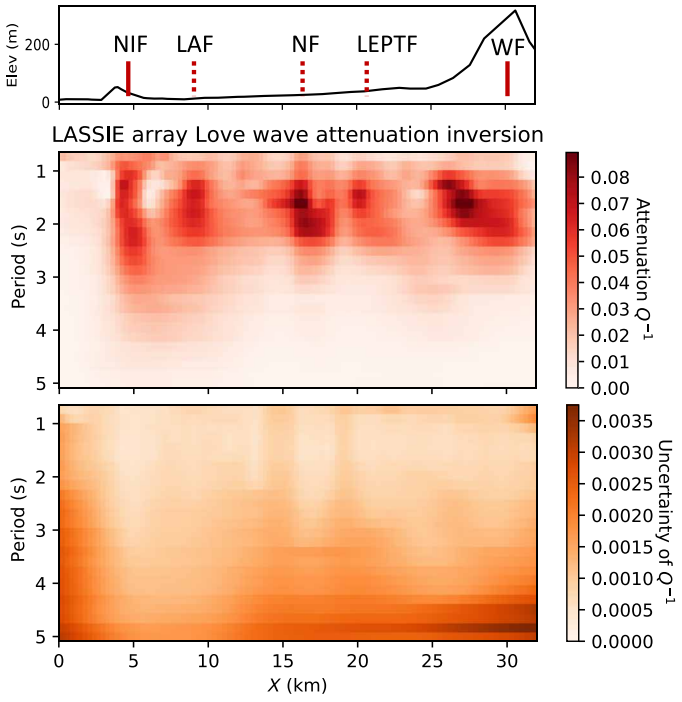

Fig. 2. Love wave attenuation inversion with uncertainty quantification. Top: Topography along the A-A′ profile of the LASSIE array. Middle: Love wave 1/*Q* attenuation tomography with period between 0.74 and 5.0 s. Bottom: Uncertainty quantification showing 1 SD for 1/*Q*. Solid line: fault with surface trace. Dashed line: blind faults. NIF, Newport-Inglewood fault; LAF, Los Alamitos fault; NF, Norwalk fault; LEPTF, lower Elysian Park thrust fault.

The estimated Love wave attenuation 1/*Q* values appear to reflect with known fault zones in the Los Angeles basin (Fig. 2). Specifically, the Newport-Inglewood fault correlates with a thin vertical stripe at ~5-km location with strong attenuation 1/*Q* ~ 0.06 that extends between the periods of 0.74 and 3.0 s. The other three blind faults, the Los Alamitos fault, the Norwalk fault, and the lower Elysian Park thrust fault, span narrower period ranges, suggesting that these faults are confined to a narrower depth range in the near surface compared with the Newport-Inglewood fault.

We propagate the uncertainty of Q_{23} to the estimated Love wave attenuation tomography 1/*Q* values through the linear ridge regression (text S3). The uncertainty is displayed as 1 standard deviation (SD) of the inverted 1/*Q* value. The estimated uncertainty level (Fig. 2) indicates that most of the attenuation tomography 1/*Q* results are well constrained from 0.74- to 4.0-s periods. Some attenuation 1/*Q* values are only two to five times their SD at the southwest tip (~0.1 km) of the LASSIE array. The attenuation structure using periods greater than 4.2 s between 12 and 32 km horizontally is poorly constrained due to the longer wavelength and the resulting more subtle amplitude decay for the same distances.

Shear attenuation depth conversion and interpretations

We need a shear velocity model beneath the LASSIE array to convert the Love wave attenuation at different periods to shear attenuation at depth. For this purpose, we perform Love wave phase velocity tomography using differential travel times from similar combinations of station triplets as used in attenuation tomography (fig. S1) because the differential time measurements considerably reduce the bias due to uneven noise source distribution (*18*). We convert the Love wave phase velocity tomography images to a shear velocity model as a function of depth (text S4) with the traditional perturbation-based approach (*19*). The shear velocity model (Fig. 3A) shows a smoothly varying lateral velocity structure between 0- and 26-km locations along the LASSIE array, indicating similar site responses for nearby receiver locations.

We apply a linear least-squares inversion to the shear attenuation depth profile estimation (*20*). For each horizontal grid location along the LASSIE array, we discretize the one-dimensional (1D) depth

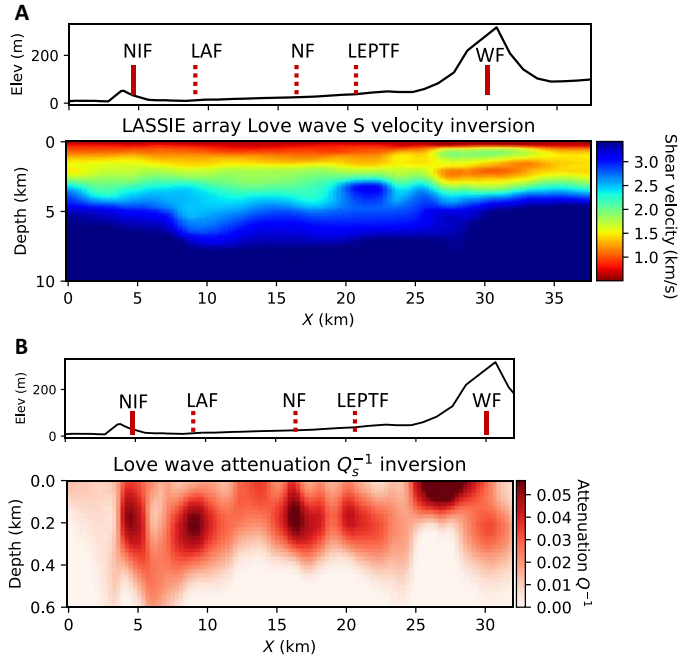

Fig. 3. Depth conversion for attenuation structure. Shear (S) wave (**A**) velocity and (**B**) attenuation tomography based on Love wave. Fault acronyms are the same as in Fig. 2.

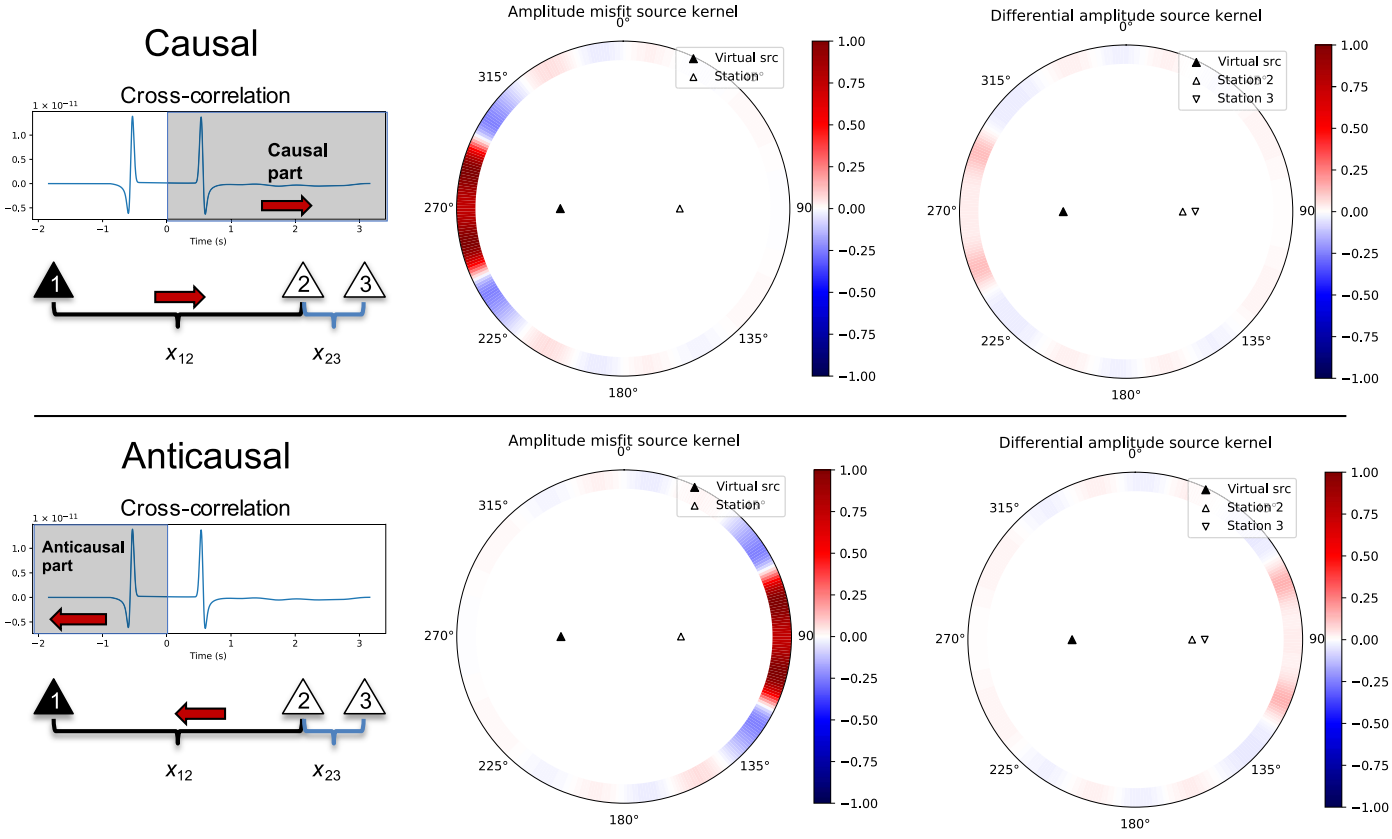

Fig. 4. Linear station triplet and cancellation of noise source sensitivity. The interstation distances are 38 and 42 km for the pairs 1-2 and 1-3, respectively. The top panel applies to the causal part of cross-correlation function while the bottom panel applies to the anticausal part. Columns 1, 2, and 3 correspond to triplet geometry, amplitude source kernel, and amplitude ratio (differential logarithmic amplitude) source kernel, respectively.

grid beneath it using 0.04-km grid spacing for a depth range between 0 and 2 km and 0.2-km grid spacing for a depth range between 2 and 5 km. We then estimate the shear attenuation in the *l*th depth layer $1/Q_{\beta l}$ from the Love wave attenuation $1/Q_L$ through a linear least-squares inversion using Love wave phase velocity sensitivity kernels (text S4).

The shear attenuation result (Fig. 3B) shows that the Newport-Inglewood fault correlates with a low-*Q* 1-km-wide band extending from the surface to ~0.4-km depth, below which the resolution of surface waves deteriorates. The Los Alamitos fault corresponds to a low-*Q* patch defined between 0.05 and 0.4 km in depth and 7 and 11 km horizontally, which agrees with the lack of surface rupture. The depth of fault tip can potentially constrain the recency of fault motion, which cuts through the Harbor stratum but not the Mesa stratum according to stratigraphy data from a nearby site at Long Beach City College (*21*). According to the dated ages of different stratigraphic units, the recency of faulting estimate for the Los Alamitos fault is between 80,000 and 160,000 years, which is considerably narrower than the previous age bracket between 11,000 and 500,000 years (*22*). The location of the Norwalk fault was poorly constrained previously, but we find an asymmetric low-*Q* patch between 16 and 18 km horizontally that matches its location. The upper tip of the Norwalk fault is much closer to the surface than the Los Alamitos fault, suggesting that it may be more recently active. The lower Elysian Park thrust corresponds to an asymmetric patch between 19.5 and 23 km horizontally with a weaker attenuation of $Q \sim 30$, suggesting that it contains less damage in the near-surface structure.

A low-*Q* anomaly between 25 and 28 km (Fig. 3B) horizontally and, in the top, 0.1-km depth does not correspond to any known fault. We believe that this anomaly is likely produced by the hill of ~300-m elevation spanning between 25 and 34 km in the *X* direction. At a much larger scale, surface topography is known to affect surface wave amplitude according to a study north of the Los Angeles basin (*23*), in which the San Gabriel Mountains reduce the peak surface wave amplitude.

DISCUSSION

The near-surface attenuation result contains strong lateral variability that can be used to model site-specific future earthquake ground motions in the Los Angeles basin. Because the attenuation model does not simply correlate with the velocity model, shear attenuation tomography provides additional information, in particular potentially a stronger sensitivity to fault zone structure. The method of ambient noise attenuation tomography using linear dense array can be generalized to 2D arrays of different length scales, as long as surface topography is negligible compared to the target depth range. In particular, this improved approach may facilitate the detection and location of near-surface blind faults in populated/urban sedimentary basins around the world where strong attenuation positively correlates with cracks and pore fluids in a fault zone damage structure (*24*).

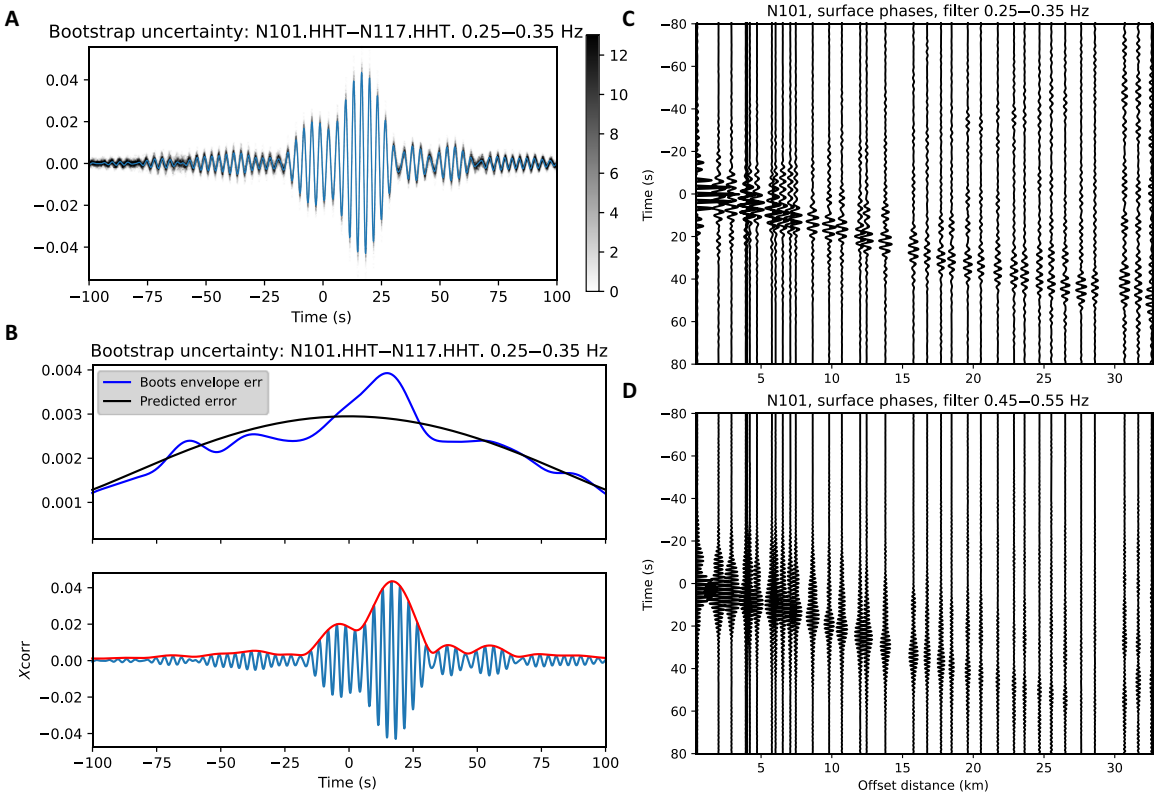

Fig. 5. Uncertainty quantification and amplitude measurements. (**A**) and (**B**) are narrowband filtered noise cross-correlation bootstrap distribution and amplitude uncertainty, respectively. (**C**) Virtual source N101 waveform gather filtered between 0.25 and 0.35 Hz. (**D**) Virtual source N101 waveform gather filtered between 0.45 and 0.55 Hz.

We improve the previous attenuation inversion technique using a linear triplet of stations by imposing a limit on maximum 25% difference between the distances for two pairs of stations when measuring the amplitude ratio. Interstation distance and wavelength determine the angular width of the Fresnel zone (*18*, *25*), where the noise sources have constructive interference. The goal of the distance limit is to facilitate cancellation of noise source sensitivity within the Fresnel zone after taking amplitude ratio by ensuring the maximum overlap of the Fresnel zones for the two pairs of stations (Fig. 4). Detailed derivation for finite-frequency amplitude source kernels is included in text S5.

It is important to understand the limitation of attenuation tomography based on ambient noise interferometry. There are potential competing factors including elastic scattering due to fault zone or fold structure, notable topography compared to wavelength and depth of interest, human infrastructure with deep foundations, and anthropogenic noise sources. The elastic wave propagation effect due to heterogeneous medium can cause focusing/defocusing of surface wave amplitudes, which is not addressed here due to the limitation of the 1D linear array. Substantial topography can introduce artifacts in surface wave amplitude and we avoid interpretation for attenuation/velocity structure beneath a hill overlaying the Whittier fault. As is true for many attenuation studies, the current technique cannot separate scattering attenuation from intrinsic attenuation. Undesirable urban noise can contaminate the amplitude information derived from ambient noise interferometry. Despite these limitations, the coincidence between attenuation tomography and known local faults shows the promise of this improved method and motivates further studies.

MATERIALS AND METHODS

Liu *et al.* (*13*) developed the attenuation inversion technique for linear triplet of stations, and Allmark *et al.* (*17*) extended it to a real-world tomographic application for a 2D dense array in the North Sea with an interpretation in terms of basin fracture properties. Here, we introduce a new criterion on enforcing the similar distances for two pairs of stations within the triplet when taking amplitude ratios to reduce noise source sensitivity further. In addition, we convert the Love wave attenuation to shear attenuation at different depths through the Anderson *et al.* (*20*) theory.

We download the LASSIE array continuous data between the Julian days 274 to 300 of 2014 consisting of 42 broadband seismometers along a line A-A′ (Fig. 1). We remove instrument response from the three-component sensors and downsample the data from 100 to 10 Hz. We divide the continuous noise data into evenly spaced 50-s time windows with 10-s gaps between neighboring windows. We then cross-correlate the corresponding time windows from two sensors in the frequency domain and estimate the statistics of the cross-spectral values between 0.1 and 5.0 Hz. For each frequency, a cross-spectrum is marked as an outlier if it exceeds four times the median absolute deviation. Any time window with more than 10% outliers between 0.1 and 5.0 Hz is excluded from subsequent analysis and stacking (*26*, *27*).

The core of the attenuation inversion method is based on linear triplets of seismic stations (*13*, *17*, *28*), which act to cancel common noise sources' contributions by taking amplitude ratios between two pairs of stations (text S5). For the causal part of noise cross-correlation function (Fig. 4, top), the amplitude measurement of station pair 1-2 is very sensitive to noise sources within the Fresnel zone (red) on the left. Given that the interstation distances for the two station pairs 1-3 (42 km) and 1-2 (38 km) are similar, the amplitude ratio (differential logarithmic amplitude) measurement is insensitive to noise sources within the Fresnel zone. Similarly, for the anticausal part of the noise cross-correlation function (Fig. 4, bottom), the amplitude ratio measurement of the pairs 1-3 and 1-2 shows substantially reduced sensitivity to noise sources within the Fresnel zone on the right as compared to the source sensitivity of amplitude measurement for the pair 1-2. On the basis of the finite-frequency source kernels for amplitude ratio measurements, a satisfactory cancellation of the sensitivity to noise sources within the Fresnel zone requires that the two pairs of stations have similar interstation distances such that the Fresnel zones of the two pairs will largely overlap (*18*). Therefore, we only select the station triplet where the distance x_{23} of the two nearby stations is less than 25% of the distance to the virtual source x_{12}.

The linear triplet inversion can be formulated for two scenarios. In the first case, the virtual source emits waves recorded by receivers 2 and 3 as the causal part of interferometric functions 1-2 and 1-3. The linear least-squares inversion based on amplitude ratios yields the attenuation quality factor Q_{23} between 2 and 3

$$\ln \widetilde{C}^{+}_{13}(\omega) - \ln \widetilde{C}^{+}_{12}(\omega) = \frac{-\omega \Delta t_{23}}{2\,Q_{23}} + \ln \frac{\gamma_3}{\gamma_2} \tag{1}$$

where $\widetilde{C}^{+}_{13}$ and $\widetilde{C}^{+}_{12}$ are causal part amplitudes for the pairs 1-3 and 1-2, respectively, after correction for geometric spreading (text S1). We assume that the ratio of site amplification factors γ_3 and γ_2 is constant over a narrow frequency band. The travel time difference between receivers 2 and 3 is $\Delta t_{23} = t_{13} - t_{12}$. The natural logarithm is $\ln(\circlearrowleft)$.

In the second case, stations 2 and 3 emit waves that converge at station 1 as the receiver, which is equivalent to using the anticausal parts of noise interferometric functions for 1-2 and 1-3. The linear least-squares inversion for Q_{23} using the anticausal part of noise correlation function is

$$\ln \widetilde{C}^{-}_{12}(\omega) - \ln \widetilde{C}^{-}_{13}(\omega) = \frac{-\omega \Delta t_{23}}{2\,Q_{23}} + \ln \frac{\gamma_2}{\gamma_3} \tag{2}$$

where $\widetilde{C}^{-}_{12}$ and $\widetilde{C}^{-}_{13}$ are the anticausal part amplitudes for the pairs 1-2 and 1-3, respectively, after correction for geometric spreading.

Before applying the attenuation inversion to the LASSIE array data, the spectra of each noise cross-correlation are normalized using the same spectral normalization function, defined as the median power spectra on horizontal components among all stations. The spectral normalization step has similar effects to pre-whitening (*29*) in traditional noise preprocessing workflow, while preserving the relative amplitude information.

To extract amplitude information with uncertainty from the transverse-transverse component noise interferometric functions, we quantify uncertainty in the narrowband-filtered noise cross-correlation using both bootstrap and theoretical approaches. The amplitude is simply derived from the peak of the envelope for noise interferometry, while its associated uncertainty requires more steps. The bootstrap method approximates the variance for every discrete time point of noise the cross-correlation (Fig. 5A), by randomly resampling the noise time blocks (observations) with replacement (text S2). Each hour-long time block ensures that the temporal correlation within the time block will be preserved. The theoretical uncertainty of noise cross-correlation function is derived (text S2) from the standard errors of stacked noise cross-spectra under the assumption of a diffuse noise field. By comparing these two approaches to uncertainty quantification, we find that the bootstrap uncertainty is notably higher than the diffuse field theory predicted error for the ballistic Love wave arrival (Fig. 5B), indicating a strong nondiffuse component to the ambient seismic noise from 0.25 to 0.35 Hz. Therefore, we use the bootstrap uncertainty instead of the diffuse field theory-predicted uncertainty for peak amplitude measurements.

For the westernmost virtual source N101 of the LASSIE array, we plot its transverse component cross-correlations with all other sensors (Fig. 5, C and D). The amplitude versus distance decays more slowly for the waveforms filtered at lower frequencies between 0.25 and 0.35 Hz (Fig. 5C) than those filtered at higher frequencies between 0.45 and 0.55 Hz (Fig. 5D), which is due to more cycles of wavelengths suffered within the same distance for higher frequencies.

SUPPLEMENTARY MATERIALS

Supplementary material for this article is available at http://advances.sciencemag.org/cgi/content/full/7/22/eabe1030/DC1

REFERENCES AND NOTES

1. R. F. Yerkes, T. H. McCulloh, J. E. Schoellhamer, J. G. Vedder, Geology of the Los Angeles Basin, California; An introduction, *Professional Paper* (Report 420A, 1965).
2. T. L. Wright, Chapter 3. Structural geology and tectonic evolution of the Los Angeles Basin, California, in *Active Margin Basins*, K. T. Biddle, Ed. (American Association of Petroleum Geologists, 1991).
3. E. Hauksson, S. Gross, Source parameters of the 1933 Long Beach earthquake. *Bull. Seismol. Soc. Am.* **81**, 81–98 (1991).
4. J. H. Shaw, J. Suppe, Earthquake hazards of active blind-thrust faults under the central Los Angeles basin, California. *J. Geophys. Res. Solid Earth* **101**, 8623–8642 (1996).
5. E. Hauksson, Seismotectonics of the Newport-Inglewood fault zone in the Los Angeles basin, southern California. *Bull. Seismol. Soc. Am.* **77**, 539–561 (1987).
6. Y. Ben-Zion, Properties of seismic fault zone waves and their utility for imaging low-velocity structures. *J. Geophys. Res. Solid Earth* **103**, 12567–12585 (1998).
7. F. J. McDonal, F. A. Angona, R. L. Mills, R. L. Sengbush, R. G. Van Nostrand, J. E. White, Attenuation of shear and compressional waves in pierre shale. *Geophysics* **23**, 421–439 (1958).
8. R. E. Abercrombie, Crustal attenuation and site effects at Parkfield, California. *J. Geophys. Res. Solid Earth.* **105**, 6277–6286 (2000).
9. L. Zhou, X. Song, X. Yang, C. Zhao, Rayleigh wave attenuation tomography in the crust of the Chinese Mainland. *Geochem. Geophys. Geosystems.* **21**, e2020GC008971 (2020).
10. Z. Peng, Y. Ben-Zion, A. J. Michael, L. Zhu, Quantitative analysis of seismic fault zone waves in the rupture zone of the 1992 Landers, California, earthquake: Evidence for a shallow trapping structure. *Geophys. J. Int.* **155**, 1021–1041 (2003).
11. R. L. Weaver, On the retrieval of attenuation and site amplifications from ambient noise on linear arrays: Further numerical simulations. *Geophys. J. Int.* **193**, 1644–1657 (2013).
12. R. L. Weaver, On the amplitudes of correlations and the inference of attenuations, specific intensities and site factors from ambient noise. *Comptes Rendus Geosci.* **343**, 615–622 (2011).
13. X. Liu, Y. Ben-Zion, D. Zigone, Extracting seismic attenuation coefficients from cross-correlations of ambient noise at linear triplets of stations. *Geophys. J. Int.* **203**, 1149–1163 (2015).
14. A. Haendel, M. Ohrnberger, F. Krüger, Extracting near-surface Q_L between 1–4 Hz from higher-order noise correlations in the Euroseistest area, Greece. *Geophys. J. Int.* **207**, 655–666 (2016).
15. D. C. Bowden, V. C. Tsai, F.-C. Lin, Amplification and attenuation across USArray using ambient noise wavefront tracking. *J. Geophys. Res. Solid Earth* **122**, 10,086–10,101 (2017).
16. Y. Ma, R. W. Clayton, Structure of the Los Angeles Basin from ambient noise and receiver functions. *Geophys. J. Int.* **206**, 1645–1651 (2016).

17. C. Allmark, A. Curtis, E. Galetti, S. de Ridder, Seismic attenuation from ambient noise across the north sea ekofisk permanent array. *J. Geophys. Res. Solid Earth* **123**, 8691–8710 (2018).
18. X. Liu, Finite-frequency sensitivity kernels for seismic noise interferometry based on differential time measurements. *J. Geophys. Res. Solid Earth* **125**, e2019JB018932 (2020).
19. R. B. Herrmann, C. J. Ammon, Computer programs in seismology: Surface waves, receiver functions and crustal structure, Saint Louis University, St. Louis, MO, USA (2002).
20. D. L. Anderson, A. Ben-Menahem, C. B. Archambeau, Attenuation of seismic energy in the upper mantle. *J. Geophys. Res.* **70**, 1441–1448 (1965).
21. D. J. Ponti, K. D. Ehman, B. D. Edwards, J. C. Tinsley III, T. Hildenbrand, J. W. Hillhouse, R. T. Hanson, K. McDougall, C. L. Powell II, E. Wan, M. Land, S. Mahan, A. M. Sarna-Wojcicki, A 3-Dimensional Model of Water-Bearing Sequences in the Dominguez Gap Region, Long Beach, California, Open-File Report (Report 2007–1013, 2007), p. 38.
22. J. I. Ziony, C. M. Wentworth, J. M. Buchanan-Banks, H. C. Wagner, Preliminary map showing recency of faulting in coastal southern California, Miscellaneous Field Studies Map (Report 585, 1974).
23. S. Ma, R. J. Archuleta, M. T. Page, Effects of large-scale surface topography on ground motions, as demonstrated by a study of the san gabriel mountains, Los Angeles, California. *Bull. Seismol. Soc. Am.* **97**, 2066–2079 (2007).
24. K. W. Winkler, A. Nur, Seismic attenuation: Effects of pore fluids and frictional-sliding. *Geophysics* **47**, 1–129 (1982).
25. L. Stehly, P. Boué, On the interpretation of the amplitude decay of noise correlations computed along a line of receivers. *Geophys. J. Int.* **209**, 358–372 (2017).
26. X. Liu, G. C. Beroza, Quantifying the effects of nondiffuse noise on ballistic and coda wave amplitude from variances of seismic noise interferometry in Southern California. *J. Geophys. Res. Solid Earth* **125**, e2019JB017617 (2020).
27. X. Liu, Y. Ben-Zion, D. Zigone, Frequency domain analysis of errors in cross-correlations of ambient seismic noise. *Geophys. J. Int.* **207**, 1630–1652 (2016).
28. X. Liu, Y. Ben-Zion, Theoretical and numerical results on effects of attenuation on correlation functions of ambient seismic noise. *Geophys. J. Int.* **194**, 1966–1983 (2013).
29. G. D. Bensen, M. H. Ritzwoller, M. P. Barmin, A. L. Levshin, F. Lin, M. P. Moschetti, N. M. Shapiro, Y. Yang, Processing seismic ambient noise data to obtain reliable broad-band surface wave dispersion measurements. *Geophys. J. Int.* **169**, 1239–1260 (2007).

Acknowledgments: We appreciate the discussions with Yehuda Ben-Zion and Hongyi Li that help improve the manuscript. This paper benefited from comments of the associate editor M. Ritzwoller and four anonymous reviewers. **Funding:** The first author X.L. acknowledges support from the National Natural Science Foundation of China under grant no. U1939203. L.Y. acknowledges support from the National Key R&D Program of China (grant no. 2017YFC0601206). This work was cosupported by Southern California Earthquake Center (SCEC) grant no. 20208 as SCEC contribution 10983. SCEC is funded by the NSF cooperative agreement EAR-1600087 and USGS cooperative agreement G17AC00047. **Author contributions:** X.L. processed the data and performed attenuation/velocity inversion. G.C.B. conceived the study and contributed to the method and figures. L.Y. performed numerical simulations and interpretation discussion. W.L.E. contributed to the interpretation of the model. **Competing interests:** The authors declare that they have no competing interests. **Data and materials availability:** All data needed to evaluate the conclusions in the paper are present in the paper and/or the Supplementary Materials. The quaternary fault lines are from SCEC Community Fault Model (https://www.scec.org/research/cfm) and USGS quaternary fault database (https://doi.org/10.5066/F7S75FJM). The LASSIE array data are available on the IRIS website (https://ds.iris.edu).

Submitted 12 August 2020
Accepted 14 April 2021
Published 28 May 2021
10.1126/sciadv.abe1030

Citation: X. Liu, G. C. Beroza, L. Yang, W. L. Ellsworth, Ambient noise Love wave attenuation tomography for the LASSIE array across the Los Angeles basin. *Sci. Adv.* **7**, eabe1030 (2021).